NANO LETTERS

2008
Vol. 8, No. 1
333−339

Inherently Tunable Electrostatic Assembly of Membrane Proteins

Hongjun Liang,[†] Gregg Whited,[‡] Chi Nguyen,[†,§] Adam Okerlund,[‡] and Galen D. Stucky*,[†]

Department of Chemistry and Biochemistry, University of California, Santa Barbara, California 93106, and Genencor International, Inc., Palo Alto, California 94304

Received November 7, 2007

ABSTRACT

Membrane proteins are a class of nanoscopic entities that control the matter, energy, and information transport across cellular boundaries. Electrostatic interactions are shown to direct the rapid co-assembly of proteorhodopsin (PR) and lipids into long-range crystalline arrays. The roles of inherent charge variations on lipid membranes and PR variants with different compositions are examined by tuning recombinant PR variants with different extramembrane domain sizes and charged amino acid substitutions, lipid membrane compositions, and lipid-to-PR stoichiometric ratios. Rational control of this predominantly electrostatic assembly for PR crystallization is demonstrated, and the same principles should be applicable to the assembly and crystallization of other integral membrane proteins.

Cells and organelles inside cells use lipid membranes to differentiate themselves from the surroundings. Membrane proteins (MPs) are a class of nanoscopic entities associated with the membranes and play crucial roles for matter, energy, and information transport across the cellular boundaries. It is estimated that MPs represent 20−30% of the currently sequenced genomes[1] and are targets for about 70% of all drugs in the market.[2]

Unlike synthetic nanoparticles that can be uniformly charged by coating with ligands,[3,4] integral MPs are amphiphilic and heterogeneously charged. They possess a spatially defined hydrophobic membrane-spanning region and charged hydrophilic extramembrane domains that interact with aqueous environments of different chemical potentials and are therefore vectorially oriented. Most integral MPs need to be purified from their native membrane-embedded states by detergents before assembly. Because of the presence of detergent micelles associated with MP hydrophobic region, directional reconstitution of MPs into well-ordered two-dimensional (2D) or 3D arrays for structural and mechanistic studies as well as many in vitro applications is notoriously difficult.

Conventional approaches to assemble MPs rely primarily on the van der Waals and hydrophobic interactions. Detergent-assisted reconstitution is the most commonly used strategy.[5] The detergent molecules solubilizing MPs also rupture lipid vesicles to form detergent−lipid-mixed micelles. Selective formation of MP−lipid co-assembled arrays depends critically on the detergent removal kinetics. In general, a large number of unpredictable parameters need to be mapped out for different MPs, and the process is easily trapped within the states of unoriented or amorphous proteoliposome/detergent assemblies.[5−12] An alternative approach called lipidic cubic phase crystallization was introduced in 1996[13] where concentrated neutral lipids such as monoolein or monopalmitolein, which are expected to give a quasisolid bicontinuous cubic phase framework in the absence of MPs, were used to initiate the nucleation and growth of MP crystals.[14] This approach has been shown to crystallize a number of MPs for high-resolution structural studies.[15−19] However, the crystallization process takes weeks to accomplish due to the slow diffusion rate of MPs in the viscous media, and some MP assemblies obtained this way diffract X-rays poorly or not at all.[20] The challenges to assemble MPs greatly hamper their structural studies. Although comprehensive understandings of various fundamental cellular activities and human health problems depend on MPs structural information, it has only been solved at a rate of ∼0.2% of that of soluble proteins.[21] Much work remains to be done to harness the unique functions of MPs. Examples include biosensor design or high-throughput drug screening,[22,23] all of which require coherently ordered MPs arrays.

The urgent demands for MPs utilization and structural studies call for new assembly strategies. Tuning electrostatic interactions to assemble MPs has been largely overlooked.

* Corresponding author. Tel.: 805 893 4872. Fax: 805 893 4120. E-mail: stucky@chem.ucsb.edu.
[†] University of California.
[‡] Genencor International, Inc..
[§] Present address: Department of Chemistry and Life Science, U.S. Military Academy, West Point, New York 10996.

10.1021/nl0729173 CCC: $40.75
Published on Web 12/04/2007

Because more than 70% by weight of biological systems consist of an aqueous solution rich in electrolytes, and the extramembrane domains of MPs are characterized by various charged amino acids, we chose to study the role of electrostatic interactions for MPs assembly.[24]

A prototypical MP is PR, which is the light-driven proton pump used by marine planktons to transport protons across their cell membranes[25,26] and is postulated to function photophysiologically for global energy and matter transformations.[25−28] Attempts to assemble PR for structural studies using conventional methods have not yet succeeded. We recently described a rapid cooperative assembly process directed by electrostatic interactions to organize PR with cationic lipids (CLs) into long-range-ordered arrays.[24] The electrostatic interactions between PR ($\sim 2 \times 3 \times 5$ nm^3) and oppositely charged CLs rapidly assembled PR into lipid bilayers to form highly ordered 2D PR crystalline lamellae (~ 5 nm $\times$ μm^2) while "squeezing out" the associated detergents spontaneously; individual crystalline lamellae were unidirectionally coupled in the transmembrane dimension to form 3D multilamellar structures ($\sim \mu$m^3) directed by the heterogeneously charged PR extramembrane domains on both sides of the lamellae.[24] We proposed a charge density matching mechanism to explain the assembly behavior.[24] Externally tunable variables, such as pH and electrolyte binding, changed the charge density of PR extramembrane domains and induced polymorphic phase transformation from a closely stacked multilamellar structure to swollen lamellar superlattices with tunable interlamellar spacing and eventually decoupled PR 2D crystals.[24]

These preliminary studies suggested that electrostatic control might be a new generic approach for 2D and 3D assembly of MPs. To test this hypothesis, we investigate here how the CL-PR assembly behavior responds to the inherent charge variations introduced by tuning both the lipid membrane and PR compositions. In addition to the recombinant PR BAC31A08 variant with a long polyhistidine tail (long-His PR),[24] three other PR variants with different extramembrane domain sizes and charged amino acid substitutions are designed and examined (charge-mutated long-His PR, short-His PR, and no-His PR. See Supporting Information for PR sequence, nomenclature, mutagenesis, expression and purification). We observe essentially the same assembly behavior for the different PR variants, only that the pH boundaries for the phase transitions are shifted due to the changes in PR compositions. This strongly suggests that the electrostatic assembly is independent of specific MP sequence and might be used to assemble other integral MPs. To fine-tune the electrostatic assembly, charge heterogeneities on lipid membranes are also introduced by varying membrane compositions and lipid-to-PR stoichiometric ratios (L/P ratios. L and P represent the total number of lipids and PR in the system, respectively). The modulation of membrane charge density is shown to further shift the pH boundaries for the phase transitions. Positional correlation of PR in adjacent lamellae is possible, and formation of PR 3D crystals is observed when the electrostatic assembly is appropriately tuned by a combination of externally induced and inherent charge variations on the assembling components (Figure 1).

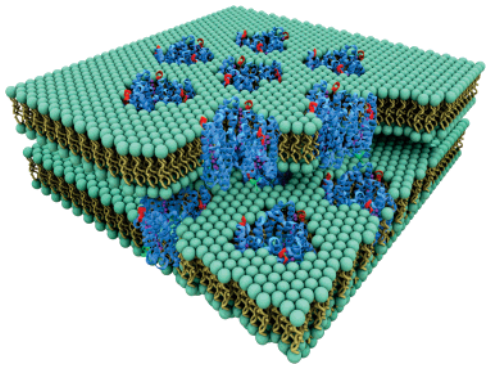

Figure 1. Schematic representation of the electrostatic assembly of PR and CLs. Nanoscopic PR trimers solubilized by *n*-dodecyl β-D-maltoside (DDM) are spontaneously co-assembled with oppositely charged small CL amphiphiles to form 2D PR crystalline lamellae. Different lamellae are unidirectionally coupled to form 3D long-range-ordered arrays. Formation of 3D PR "ionic" crystals as a result of positional correlation of PR in adjacent lamellae is possible when the electrostatic assembly is appropriately tuned by a combination of externally induced and inherent charge variations on the assembling components. The top layer of the 3D assembly is cut open to demonstrate the membrane-embedded state of PR. The DDM molecules originally associated with the PR hydrophobic domain are "squeezed out" (not shown) during the assembly process. The C- and N-terminus of PR are shown as red and green, respectively. The retinal chromophore in PR is shown as purple.

Short-His PR. We examined the assembly behavior of CLs with short-His PR, which has a polyhistidine tail on the cytoplasma (CP) side that is 22 amino acids shorter than the long-His PR reported before.[24] It has been shown that the size of the hydrophilic extramembrane domains is critical for MPs crystallization.[29,30] The change in size also causes an altered charge state of the extramembrane domain. The pH-dependent effective charge associated with each extramembrane domain of the short-His PR as calculated based on the Henderson−Hasselbach equation[31] using the PR secondary structure model[25] is shown in Figure 2a. At pH $= 5$, the two extramembrane domains are oppositely charged with the charge density on the CP side and extracellular (EC) side $+8/S$ and $-2/S$, respectively, where S represents the cross-section area of the protein. In contrast to the long-His PR, the heterogeneously charged short-His PR does not have a well-matched charge density on its extramembrane domains. Instead of forming a closely stacked multilamellar structure as the assembly of long-His PR and CLs at this pH,[24] a loosely stacked multilamellar structure appears. Typical synchrotron small-angle X-ray scattering (SAXS) of the proteoliposome assemblies comprised of short-His PR and CLs is shown in Figure 2c (See Supporting Information for the experimental details on the preparation of proteoliposome assemblies). The peaks marked by black arrows on each curve are the harmonics of the lamellar correlations. The lamellar periodicity is 64.1 Å ($q_{001} = 0.098$ Å^{-1}, top curve, 100% DOTAP), which is expanded by $\sim$10 Å from the closely stacked multilamellar structure.[24] The loosely stacked lamellar structure is further confirmed by transmis-

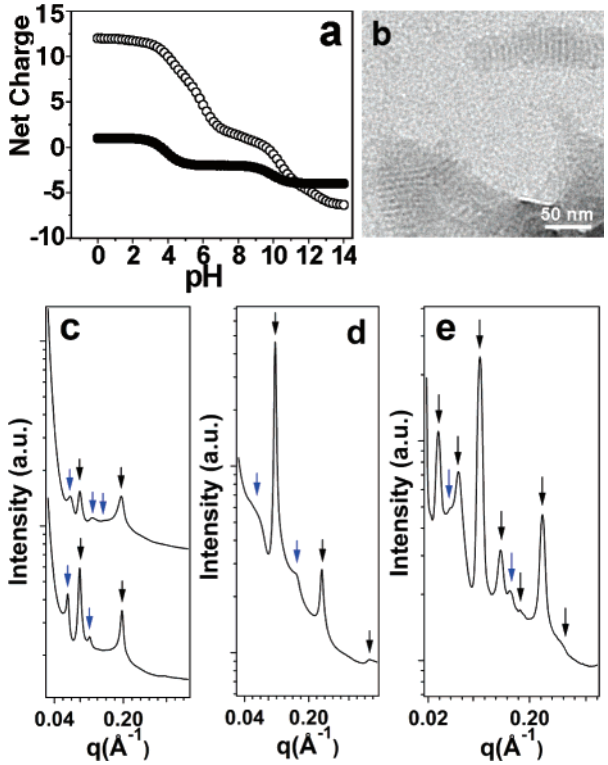

Figure 2. Electrostatic assembly behavior of short-His PR and CLs. (a): pH-dependent charging states of the two PR extramembrane domains (●, EC side; ○, CP side). (b) TEM of CL-PR assemblies stained with UA (100% DOTAP, L/P = 20, pH = 5) shows loosely stacked multilamellar structure. (c) Synchrotron SAXS of CL-PR assemblies assembled at pH = 5, where the two extramembrane domains are oppositely charged but with an unbalanced charge density. Top curve: 100% DOTAP, L/P = 20. Bottom curve: 30/70 DOTAP/DOPC, L/P = 60. Peaks under black arrows are harmonics of a loosely stacked multilamellar structure, peaks under blue arrows are correlations of the in-membrane PR 2D hexagonal lattice. (d) Synchrotron SAXS of CL-PR assemblies assembled at pH = 7.5 (100% DOTAP, L/P = 60), where the two extramembrane domains are oppositely charged with charge density matching. Peaks under black arrows reveal a closely stacked multilamellar structure, peaks under blue arrows are from in-membrane PR correlations. (e) In-house SAXS of CL-PR assemblies assembled at pH = 10 (30/70 DOTAP/DOPC, L/P = 60), where both extramembrane domains are slightly anionically charged. Up to seven Bragg harmonics from a lamellar superlattice (peaks under black arrows) and weak correlations from PR in each membrane layer (peaks under blue arrows) are observed.

sion electron microscopy (TEM) (Figure 2b). Proteoliposome assemblies stained by uranium acetate (UA) show equally spaced strips with a periodicity ~68 Å, which agrees well with the expanded lamellar periodicity revealed by SAXS, but is ~12 Å more than that observed for the closely stacked lamellar structure.[24]

The short-His PR has a significant shorter tail on the CP side of the extramembrane domain than the long-his PR, thus a smaller dimension spanning along its transmembrane direction is expected. But the lamellar periodicity of the CL-PR assemblies is counter-intuitively larger, which unambiguously confirms that the charge density matching between the extramembrane domains of PR in adjacent layers plays a decisive role, and the spontaneous assembly process in this system is guided by the electrostatic interactions rather than the van der Waals interactions proportional to the size of PR extramembrane domains.[29,30] The PR in-layer order is also affected by the interplay of electrostatic interactions. Unlike the 2D rectangular PR lattice formed in the closely stacked multilamellar structure,[24] a 2D hexagonal PR lattice appears at this pH (Figure 2c, peaks marked by blue arrows). For 30/70 DOTAP/DOPC membrane, two peaks at 0.071 and 0.122 Å^{-1} are observed (bottom curve), corresponding to q_{10} and q_{11} of a 2D PR hexagonal lattice with a unit cell of 102.1 Å; for 100% DOTAP membrane, three peaks at 0.076, 0.130, and 0.153 Å^{-1} are observed (top curve), corresponding to q_{10}, q_{11}, and q_{20} of a 2D PR hexagonal lattice with a unit cell of 95.4 Å.

When pH is raised to 7.5, the two extramembrane domains of short-His PR are still oppositely charged but with a more balanced charge density. The charge density is $\sim +2/S$ on CP side and $-2/S$ on EC side, respectively. The interlayer PR−PR charge density matching is satisfied. A closely stacked multilamellar structure like that observed for the assembly of long-His PR with CLs at pH = 5 appears, in contrast to the lamellar superlattice structure that appeared in the assembly of long-His PR and CLs around this pH.[24] Typical synchrotron SAXS of the proteoliposome assembly comprised of short-His PR and 100% DOTAP at pH = 7.5 is shown in Figure 2d. The three equally spaced harmonics marked by black arrows reveal a closely stacked lamellar structure with a lamellar periodicity of 53.7 Å (q_{001} = 0.117 Å^{-1}). The in-layer PR correlations are marked by blue arrows.

The transition from the stacked lamellar to lamellar superlattice structure[24] does appear when pH is further raised to 10, where both extramembrane domains of PR are anionically charged. Typical in-house SAXS is shown in Figure 2e. Up to seven orders of equally spaced Bragg diffraction peaks marked by black arrows reveal a lamellar superlattice structure with a periodicity of 169.7 Å (q_{001} = 0.037 Å^{-1}). The in-layer PR correlations are observed (marked by the blue arrows), but higher resolution SAXS is needed to identify its symmetry. Like the assemblies comprised of long-His PR and CLs, disintegration of this 3D lamellar superlattice occurs when both extramembrane domains of PR are more anionically charged by further raising the pH.

We observe essentially the same phase transition behavior as the assembly of long-His PR with CLs[24] while short-His PR is used, only that the pH boundaries for the phase transition are shifted because the absence of the 22 charged hydrophilic chain drastically changes the pH-dependent charge density of the extramembrane domain of PR. This observation suggests that the 3D unidirectional coupling of the 2D proteoliposome crystalline lamellae is primarily defined by the electrostatic interaction between PR extramembrane domains resting on top of the adjacent layers.

No-His PR and Charge-Mutated Long-His PR. Further evidence of the inherently tunable electrostatic nature of the assembly comes from studies of two other PR mutants. In fact, PR without the presence of the extra hydrophilic polyhistidine tail at all follows similar assembly behavior.

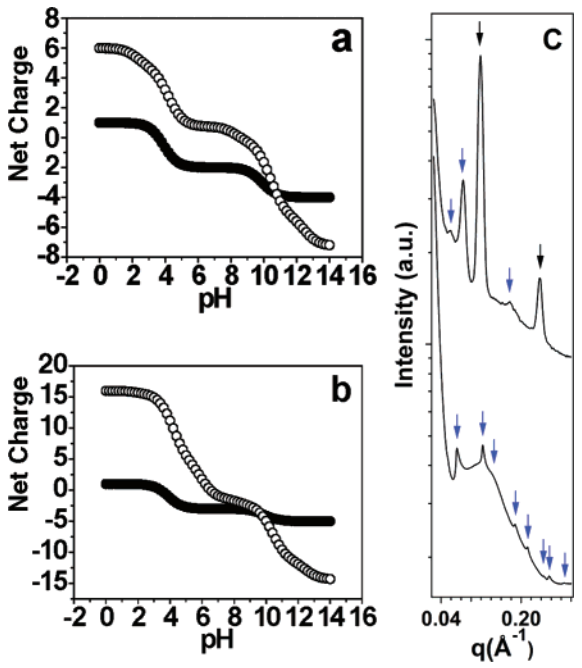

Figure 3. Typical electrostatic assembly behavior of no-His PR and charge-mutated long-His PR. (a) pH-dependent charging states of the two extramembrane domains of no-His PR (●, EC side; ○, CP side). (b) pH-dependent charging states of the two extramembrane domains of charge-mutated long-His PR (●, EC side; ○, CP side). (c) Top curve: in-house SAXS of CL-PR assemblies comprised of no-His PR and 100% DOTAP assembled at pH = 7.0 (L/P = 60), where the two extramembrane domains of PR are oppositely charged with relatively balanced charge density. Correlations from a closely stacked multilamellar structure (peaks under black arrows) with 2D PR rectangular lattice in each stacking layer (peaks under blue arrows) are clearly observed. Bottom curve: synchrotron SAXS of CL-PR assemblies comprised of charge-mutated long-His PR and 100% DOTAP assembled at pH = 7.5 (L/P = 40), where both extramembrane domains of PR are strongly anionically charged. The peaks under blue arrows are a complete set of the first eight diffractions from 2D PR crystals with a hexagonal symmetry.

The pH-dependent effective charge associated with each extramembrane domain of the no-His PR is shown in Figure 3a. In Figure 3c, the top curve is an example of the in-house SAXS for the CL-PR assemblies assembled at pH = 7, where the two extramembrane domains are oppositely charged with fairly matched charge density ($\sim +1/S$ on CP side and $-2/S$ on EC side, respectively). A closely stacked lamellar structure induced by charge density matching appears as expected. The peaks marked by black arrows are the first and second Bragg diffraction of the multilamellar assemblies. The lamellar periodicity is 52.8 Å ($q_{001} = 0.119$ Å^{-1}), which is ~2 Å smaller than the lamellar periodicity of the closely stacked CL-PR assemblies in which the long polyhistidine tail on PR is present.[24] The peaks under blue arrows are at 0.059, 0.084, and 0.178 Å^{-1}, corresponding to the q_{10}, q_{01}, and q_{12} scattering of a 2D rectangular PR in-membrane lattice.

Besides changing the size of PR extramembrane domains, it is also possible to shift the pH boundaries of the CL-PR assemblies phase transition by site-directed mutagenesis that selectively introduces charged amino acids into PR extramembrane domains. In one example, we introduced one basic amino acid (S55R) on CP side and one acidic amino acid (G213D) on EC side in the extramembrane domain of the long-His PR. The pH-dependent effective charge associated with each extramembrane domain of the charge-mutated long-His PR is shown in Figure 3b. Compared with the long-His PR without charge mutations,[24] the G213D mutation significantly increases the anionic charges on EC side. We found that a bacteriorhodopsin purple membrane-like 2D PR crystal, which usually forms when the long-His PR and CLs are assembled at pH = 9,[24] appears for the charge-mutated long-His PR at pH = 7.5, where the interlayer PR−PR repulsion is already strong enough to decouple 3D lamellar stacking due to the increased charge density of the anionically charged extramembrane domains (bottom curve, Figure 3c). The peaks under blue arrows are at 0.072, 0.124, 0.143, 0.189, 0.214, 0.247, 0.257, and 0.286 Å^{-1}, corresponding to q_{10}, q_{11}, q_{20}, q_{21}, q_{30}, q_{22}, q_{31}, and q_{40} of a 2D hexagonal PR lattice, respectively. The diffuse peak centered at ~0.13 Å^{-1} is likely the form factor from PR and lipid vesicles.[24] Interestingly, as few as one amino acid mutation could drastically change the pH-dependent charge density of the extramembrane domains. For applications based on MP assembly, this strategy is especially useful to obtain desired CL-PR structures when wild type MP is only stable in certain pH range, where the charge density of its extramembrane domains is not able to induce the electrostatic assembly of these structures.

Modulation of Membrane Charge Density. Besides tuning the PR−PR electrostatic interaction by varying the charge density of PR extramembrane domains, the PR-membrane electrostatic interaction is tuned by diluting the cationic DOTAP membrane with zwitterionic DOPC component. For cationic membranes consisting of 100% DOTAP, the membrane charge density is always homogeneous, but when the binary mixture of DOTAP and DOPC is used, the membrane charge density may become heterogeneous at a given membrane composition. The reason lies that in CL-PR assemblies charged extramembrane domains of PR decorate a charged membrane surface, and electrostatic interactions between PR and the charged DOTAP component can induce lateral phase separation of the binary lipid membranes at the vicinity of the membrane-embedded PR. The heterogeneous lipid microdomain formation will give rise to the heterogeneous membrane charge density. The electrostatic interactions in the system are fine-tuned as a consequence, and phase transitions of CL-PR assemblies may occur.

Heterogeneous lipid microdomains within biological membranes play important roles for many cellular processes.[32,33] For example, they have been shown to modulate MP activity.[34] However, directly probing the microdomains locally (<100 nm) is difficult.[35] Using synchrotron SAXS, we study the heterogeneous lipid microdomain formation and the corresponding structural evolution of CL-PR assemblies. We vary the L/P ratios at a given membrane composition to induce the formation of heterogeneous lipid microdomains that are phase separated differently. A typical synchrotron

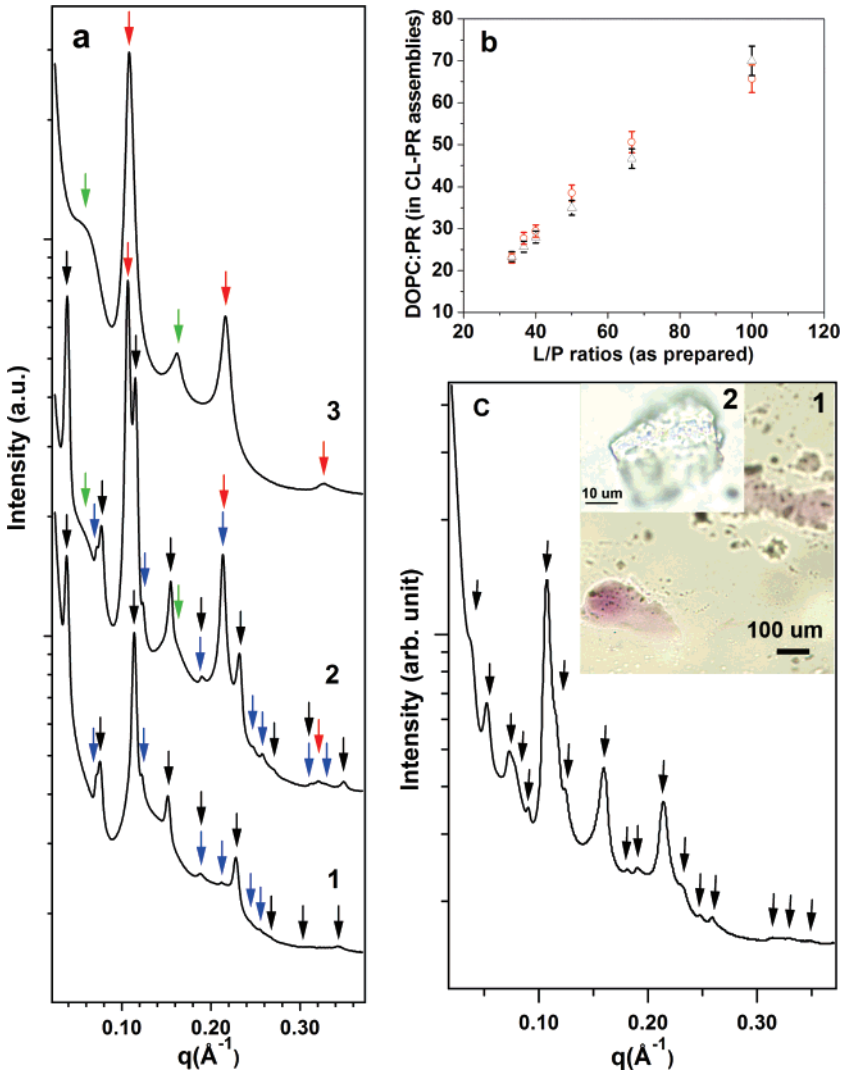

Figure 4. 3D structures of CL-PR assemblies respond to charge heterogeneities on lipid membranes. (a) Synchrotron SAXS studies of CL-PR assemblies (long-His PR with 30/70 DOTAP/DOPC, pH = 7) at different L/P ratios reveal that membrane surface charge heterogeneities play an important role to define the phase transition boundaries. Curve 1: L/P = 40. Nine equally spaced harmonics from a lamellar superlattice (marked by black arrows) and the first six correlations from an in-membrane PR 2D hexagonal lattice (marked by blue arrows) appear. Curve 2: L/P = 50. Locally enriched DOTAP microdomains at the vicinity of PR extramembrane loops start to form and initiate the formation of a closely stacked multilamellar phase, as indicated by the appearance of three new equally spaced harmonics (marked by red arrows) and new in-membrane PR correlations (marked by green arrows). Curve 3: L/P = 70. Single phase of closely stacked multilamellar CL-PR assemblies appears. (b) Comparison of the measured DOPC-to-PR stoichiometric ratios (○) in CL-PR assemblies with that to be expected if the binary mixture of zwitterionic DOPC and cationic DOTAP molecules are co-assembled proportionally with PR (△). They agree with each other, indicating the macroscopic binary lipid composition in CL-PR assemblies remains unchanged. (c) Synchrotron SAXS of PR 3D crystalline assemblies ((long-His PR with 30/70 DOTAP/DOPC, pH = 5, L/P = 67). All the peaks marked under black arrows can be indexed as diffractions from PR crystals with cubic symmetries. Inserts 1 and 2: 5× and 100× optical microscopy pictures of the CL-PR crystalline assemblies, respectively.

SAXS of CL-PR assemblies comprised of long-His PR and mixed cationic membranes at different L/P ratios is shown in Figure 4a. The solution pH is kept at 7, where both extramembrane domains of PR are slightly anionically charged.

When the L/P is 40 (Figure 4a, curve 1), up to nine equally spaced harmonics (peaks under black arrow) originated from a lamellar superlattice with a periodicity of 165.3 Å (q_{001} = 0.038 Å^{-1}) are observed. Peaks marked by the blue arrows are at 0.071, 0.123, 0.188, 0.213, 0.246, and 0.256 Å^{-1}, corresponding to the q_{10}, q_{11}, q_{21}, q_{30}, q_{22}, and q_{31} correlations of a 2D in-membrane PR hexagonal lattice, respectively.

When the L/P ratio is increased (L/P = 50, Figure 4a, curve 2), local lateral lipid phase separation, which is presumably caused by the enrichment of cationic DOTAP around the anionically charged PR extramembrane domains, starts to modulate the charge density of the membrane, and consequently the phase of CL-PR assemblies. The locally enriched DOTAP microdomains not only offset the anionic charges on PR extramembrane loops, but also enhance the PR-membrane electrostatic attraction, both of which change the delicate balance to keep the lamellar superlattice structure. In fact, a closely stacked multilamellar structure with a periodicity of 58.1 Å (q_{001} = 0.108 Å^{-1}) starts to form, as indicated by three equally spaced Bragg harmonics (peaks under red arrows); in each stacking layer, new correlations corresponding to the transformed PR 2D lattice are observed

as the weak humps marked by green arrows. This closely stacked lamellar phase coexists with the lamellar superlattice phase characterized by nine lamellar harmonics (peaks under black arrows) and a series of correlations from the 2D in-membrane PR hexagonal lattice (peaks under blue arrows).

When the L/P is further increased and more cationic DOTAP is available in the system (L/P = 70, Figure 4a, curve 3), the lamellar superlattice completely disappears, and a single phase of the closely stacked multilamellar CL-PR structure remains. Interestingly, when pH is raised and the charge density of the anionic extramembrane domains of PR increases as a result, a reverse transition from the closely stacked lamellar phase to the lamellar superlattice phase occurs, which demonstrates that the charge density of the membrane and that of the PR extramembrane domains work synergistically to define the phase transition boundaries of CL-PR assemblies.

Tuning the relative ratios of the oppositely charged assembly components available in the system at a given binary membrane composition causes the shift of the phase transition boundaries of CL-PR assemblies. Such shift is attributed to the formation of heterogeneous microdomains that modulate membrane charge density locally. Because the phospholipid DOPC component can be accurately determined by the phosphorus assay,[36,37] the DOPC-to-PR stoichiometric ratios in CL-PR assemblies are measured (see Supporting Information). These ratios are compared to that preset initially to infer whether macroscopic membrane composition changes occur after the coassembly of lipids with PR. For preset L/P ratios ranging from 30 to 100 during which CL-PR phase transition is observed, the DOPC-to-PR stoichiometric ratios in CL-PR assemblies are as the same as that to be expected if the binary mixture of zwitterionic DOPC and cationic DOTAP molecules are coassembled proportionally with PR (Figure 4b). In other words, the cationic DOTAP component from the binary liposome does not preferentially coassemble with PR than the zwitterionic DOPC component, and the membrane composition in CL-PR assemblies does not deviate from that of the initial liposome solution. This result strongly suggests that the CL-PR phase transition is caused by the local heterogeneous lipid microdomain formation within binary lipid membranes rather than macroscopic lipid phase separation.

The surface charge heterogeneities induced by charged PR extramembrane domains effectively tune the structure of CL-PR assemblies even when the macroscopic membrane composition and the effective charges associated with PR extramembrane domains are kept unchanged. Recent theoretical work on the cationic-anionic co-assembly of cylindrical objects showed that the cooperative organization is critically dependent on surface charge heterogeneities that strongly interact through polarization of the domains.[38] In addition to modifying the phase transition boundaries that define how different PR 2D lamellae are correlated, the inherently tunable surface charge heterogeneities on lipid membranes also play crucial roles for inducing positional correlations of PR in adjacent lamellae, which ultimately lead to 3D crystallization of PR. Although the 3D positional correlations of PR are generally absent when individual PR crystalline lamellae are stacked via the charge density matching mechanism, they do appear as long as appropriate surface charge heterogeneities of the membranes are obtained by tuning L/P ratios. A typical synchrotron SAXS of the 3D CL-PR "ionic" crystalline assemblies is shown (Figure 4c). All of the powder-averaged diffraction peaks (marked under black arrows) can be indexed as reflections from the PR crystalline assemblies with cubic symmetries.[39] The first peak (q_{100}) is at 0.037 $Å^{-1}$, corresponding to a cubic unit cell of 17 nm. Most of the crystalline assemblies have sizes of a few microns (Figure 4c, insert 1). Larger crystalline assembly ($\sim 10^1$ μm) with well-defined cubic geometry is also visible (Figure 4c, insert 2).

In summary, this work demonstrates that: (i) Polymorphism of the 3D electrostatic assembly consisting of the nanoscopic PR and small amphiphilic lipids are inherently tunable. The charge density of PR extramembrane domains and that of lipid membranes work synergistically to define the phase transition boundaries. (ii) For a subset of PR assemblies, modulation of the membrane charge density by introducing charge heterogeneities on membrane surface at appropriate L/P ratios induces PR 3D positional correlations, which can be exploited to grow 3D PR "ionic" crystals suitable for structural studies. (iii) Principles to control the electrostatic assembly of PR have been demonstrated to be applicable to PR variants with different extramembrane domain sizes and amino acid sequences, suggesting this approach can be applied to the assembly and crystallization of other integral membrane proteins.

Acknowledgment. We thank Professor C. R. Safinya for helpful discussions and assistance with the synchrotron SAXS experiments. This work was supported by a UC Discovery Grant and Genencor International. Part of this work made use of facilities in the Materials Research Laboratory at UCSB, which is supported by the MRSEC Program of the National Science Foundation under Award No. DMR05-20415. Portions of this research were carried out at the Stanford Synchrotron Radiation Laboratory, a national user facility operated by Stanford University on behalf of the U.S. Department of Energy, Office of Basic Energy Sciences.

Supporting Information Available: Experimental details on preparation of different PR mutants, CL-PR assemblies, SAXS, TEM, and phosphorus assay measurements. This material is available free of charge via the Internet at http://pubs.acs.org.

References

(1) Wallin, E.; von Heijne, G. *Protein Sci.* **1998**, *7*, 1029−1038.
(2) Stahlberg, H.; Fotiadis, D.; Scheuring, S.; Remigy, H.; Braun, T.; Mitsuoka, K.; Fujiyoshi, Y.; Engel, A. *FEBS Lett.* **2001**, *504*, 166−172.
(3) Shevchenko, E. V.; Talapin, D. V.; Kotov, N. A.; O'Brien, S.; Murray, C. B. *Nature* **2006**, *439*, 55−59.
(4) Kalsin, A. M.; Grzybowski, B. A. *Nano Lett.* **2007**, *7*, 1018−1021.
(5) Rigaud, J. L.; Levy, D. *Methods Enzymol.* **2003**, *372*, 65−86.
(6) Jap, B. K.; Zulauf, M.; Scheybani, T.; Hefti, A.; Baumeister, W.; Aebi, U.; Engel, A. *Ultramicroscopy* **1992**, *46*, 45−84.

(7) Engel, A.; Hoenger, A.; Hefti, A.; Henn, C.; Ford, R. C.; Kistler, J.; Zulauf, M. *J. Struct. Biol.* **1992**, *109*, 219−234.
(8) Hasler, L.; Heymann, J. B.; Engel, A.; Kistler, J.; Walz, T. *J. Struct. Biol.* **1998**, *121*, 162−171.
(9) Rigaud, J. L.; Chami, M.; Lambert, O.; Levy, D.; Ranck, J. L. *Biochim. Biophys. Acta* **2000**, *1508*, 112−128.
(10) Remigy, H. W.; Caujolle-Bert, D.; Suda, K.; Schenk, A.; Chami, M.; Engel, A. *FEBS Lett.* **2003**, *555*, 160−169.
(11) Levy, D.; Chami, M.; Rigaud, J. L. *FEBS Lett.* **2001**, *504*, 187−193.
(12) Rigaud, J. L.; Paternostre, M. T.; Bluzat, A. *Biochemistry* **1988**, *27*, 2677−2688.
(13) Landau, E. M.; Rosenbusch, J. P. *Proc. Natl. Acad. Sci. U.S.A.* **1996**, *93*, 14532−14535.
(14) Nollert, P.; Qiu, H.; Caffrey, M.; Rosenbusch, J. P.; Landau, E. M. *FEBS Lett.* **2001**, *504*, 179−186.
(15) PebayPeyroula, E.; Rummel, G.; Rosenbusch, J. P.; Landau, E. M. *Science* **1997**, *277*, 1676−1681.
(16) Katona, G.; Andreasson, U.; Landau, E. M.; Andreasson, L. E.; Neutze, R. *J. Mol. Biol.* **2003**, *331*, 681−692.
(17) Nollert, P. *Methods* **2004**, *34*, 348−353.
(18) Cherezov, V.; Yamashita, E.; Liu, W.; Zhalnina, M.; Cramer, W. A.; Caffrey, M. *J. Mol. Biol.* **2006**, *364*, 716−734.
(19) Cherezov, V.; Clogston, J.; Papiz, M. Z.; Caffrey, M. *J. Mol. Biol.* **2006**, *357*, 1605−1618.
(20) Misquitta, L. V.; Misquitta, Y.; Cherezov, V.; Slattery, O.; Mohan, J. M.; Hart, D.; Zhalnina, M.; Cramer, W. A.; Caffrey, M. *Structure* **2004**, *12*, 2113−2124.
(21) Kim, S.; Jeon, T. J.; Oberai, A.; Yang, D.; Schmidt, J. J.; Bowie, J. U. *Proc. Natl. Acad. Sci. U.S.A.* **2005**, *102*, 14278−14283.
(22) Boxer, S. G. *Curr. Opin. Chem. Biol.* **2000**, *4*, 704−709.
(23) Castellana, E. T.; Cremer, P. S. *Surf. Sci. Rep.* **2006**, *61*, 429−444.
(24) Liang, H. J.; Whited, G.; Nguyen, C.; Stucky, G. D. *Proc. Natl. Acad. Sci. U.S.A.* **2007**, *104*, 8212−8217.
(25) Beja, O.; Aravind, L.; Koonin, E. V.; Suzuki, M. T.; Hadd, A.; Nguyen, L. P.; Jovanovich, S.; Gates, C. M.; Feldman, R. A.; Spudich, J. L.; Spudich, E. N.; DeLong, E. F. *Science* **2000**, *289*, 1902−1906.
(26) Beja, O.; Spudich, E. N.; Spudich, J. L.; Leclerc, M.; DeLong, E. F. *Nature* **2001**, *411*, 786−789.
(27) DeLong, E. F.; Karl, D. M. *Nature* **2005**, *437*, 336−342.
(28) de la Torre, J. R.; Christianson, L. M.; Beja, O.; Suzuki, M. T.; Karl, D. M.; Heidelberg, J.; DeLong, E. F. *Proc. Natl. Acad. Sci. U.S.A.* **2003**, *100*, 12830−12835.
(29) Ostermeier, C.; Michel, H. *Curr. Opin. Struct. Biol.* **1997**, *7*, 697−701.
(30) Ostermeier, C.; Iwata, S.; Ludwig, B.; Michel, H. *Nat. Struct. Biol.* **1995**, *2*, 842−846.
(31) Nelson, D.; Cox, M. M. *Lehninger Principles of Biochemistry*, 3rd ed.; Worth Publishers: New York, 2000.
(32) Mouritsen, O. G.; Jorgensen, K. *Chem. Phys. Lipids* **1994**, *73*, 3−25.
(33) Welti, R.; Glaser, M. *Chem. Phys. Lipids* **1994**, *73*, 121−137.
(34) Burack, W. R.; Yuan, Q.; Biltonen, R. L. *Biochemistry* **1993**, *32*, 583−589.
(35) Kraft, M. L.; Weber, P. K.; Longo, M. L.; Hutcheon, I. D.; Boxer, S. G. *Science* **2006**, *313*, 1948−1951.
(36) Morrison, W. R. *Anal. Biochem.* **1964**, *7*, 218-&.
(37) Petitou, M.; Tuy, F.; Rosenfeld, C. *Anal. Biochem.* **1978**, *91*, 350−353.
(38) Velichko, Y. S.; de la Cruz, M. O. *J. Chem. Phys.* **2006**, *124*, 214705.
(39) The SAXS peaks have relationship $1{:}2^{0.5}{:}2{:}5^{0.5}{:}6^{0.5}{:}8^{0.5}{:}10^{0.5}{:}11^{0.5}{:}18^{0.5}{:}24^{0.5}{:}26^{0.5}{:}33^{0.5}{:}38^{0.5}{:}45^{0.5}{:}7{:}72^{0.5}{:}80^{0.5}{:}89^{0.5}$, all of which are characteristic reflections from crystals with 3D cubic symmetries. Works to obtain well-grown PR "ionic" crystals capable for protein crystallography studies are currently pursued to identify the space group and PR structure.

NL0729173